LAWRENCE
LIVERMORE
NATIONAL
LABORATORY

LLNL-CONF-566512

Performance measurements of the DIXI (dilation x-ray imager) photocathode using a laser produced x-ray source

S. R. Nagel, M. J. Ayers, B. Felker, R. F. Smith, P. M. Bell, D. K. Bradley, G. W. Collins

July 25, 2012

2012 SPIE Conference
San Diego, CA, United States
August 12, 2012 through August 16, 2012

Disclaimer

Performance measurements of the DIXI (dilation x-ray imager) photocathode using a laser produced x-ray source

Sabrina R. Nagel[a], M.J. Ayers[a], B. Felker[a], T.J. Hilsabeck[b], T. Chung[b], R.F. Smith[a], P.M. Bell[a], D.K. Bradley[a], G.W. Collins[a], , J.D. Kilkenny[b], B. Sammuli[b], J.D. Hares[c], A.K.L. Dymoke-Bradshaw[c]

[a]Lawrence Livermore National Laboratory, 7000 East Avenue, Livermore CA, USA;
[b]General Atomics, Address, San Diego CA, USA;
[c]Kentech Instruments Ltd., Address, City, UK;

ABSTRACT

DIXI (dilation x-ray imager) will be used to characterize ICF (inertial confinement fusion) implosions on the NIF. DIXI utilizes pulse-dilation technology[1] to achieve x-ray imaging with temporal gate times below 10 ps. Time resolved x-ray measurements were conducted using the COMET laser facility at the Lawrence Livermore National Laboratory. Here we focus on some of the challenges faced by the large aperture photo cathode of the instrument and report on how to maintain a flat photo cathode as well as how the required spatial resolution of the instrument is achieved.

Keywords: gated, x-ray, imager, time dilation

1. INTRODUCTION

The performance of ICF targets relies on the symmetric implosion of DT fuel in order to form a uniform central hot spot with high enough areal density and temperature to achieve ignition.[2] Gated broadband x-ray imaging at energies exceeding 8 keV is used to diagnose temporal (t = 40 to 100 ps) and spatial histories of the implosion symmetry and hot spot non-uniformities.[3] Simulations predict features around bang time, which can only be resolved by faster gated imagers.[5] Therefore it is important to diagnose those interactions at a higher frame rate.

Here we present data for a new x-ray imaging diagnostic, DIXI (Dilation x-ray imager), designed to work at shot neutron yields of up to 10^{17}. The diagnostic uses pulse-dilation of an electron signal to achieve temporal gate times of less than 10 ps.[1] Possible uses for this technology include: measuring high energy electron transport rates in fast ignition experiments, analyzing the symmetry of late stage implosion of high energy targets and investigating burn wave dynamics for igniting targets. In each case, it will be necessary to image the hard x-ray emission source (10-40 keV).

2. WORKING PRINCIPLE

DIXI uses pulse dilation of an electron signal from a transmission Photo-Cathode (PC) to achieve the short temporal gate times. Figure 1(a) shows a diagram of DIXI indicating the main sections,

Further author information: (Send correspondence to S.R. Nagel)
S.R. Nagel: E-mail: nagel7@llnl.gov, Telephone: 1 925 422 7739

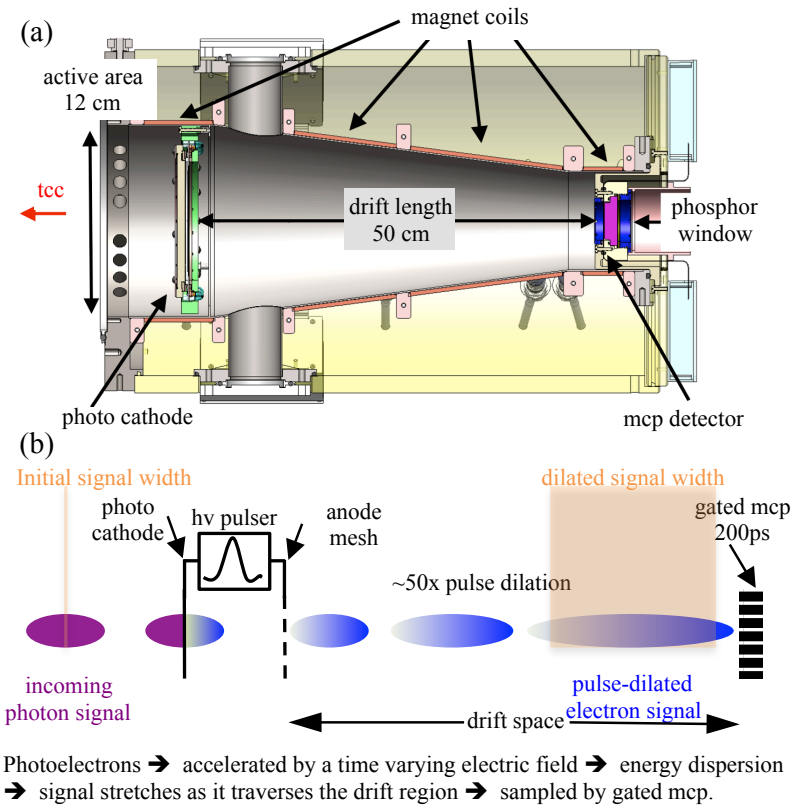

Figure 1. (a) DIXI schematic side view, optical fiber bundle and recording material not shown. (b) Working principle.

whereas (b) illustrates the working principle of the instrument. An electron signal is generated as x-rays hit the Au or CsI transmission PC.[4] The electrons are sent through a drift space in which they are kept focused by a magnetic field. The magnetic field also de-magnifies the image ($\approx 3\times$). The dilated electrons then hit the gated MCP detector, which is followed by a phosphor, fiber block and CCD/film back (fiber bundle and recording media not shown). Because the PC is pulsed, the electron signal has a velocity distribution and the electrons created early in time have a larger energy. As this pulse traverses the drift space the signal is dilated. The MCP pulse is timed relative to the PC pulse to gate the electron signal. The electron arrival time at the MCP (τ) is the sum of the electron birth time (t), and the electron drift time. The electron drift time is dependent on the voltage of the PC pulse at the time the electron is born.

$$\tau(x,y,t) = t + \frac{L_{\text{drift}}(x,y)}{v_{\text{drift}}(x,y,t)} \tag{1}$$

$$v_{\text{drift}}(x,y,t) = \sqrt{2eV_{\text{acc}}(x,y,t)/m}. \tag{2}$$

Where (x,y) is the birth location.

3. CHALLENGES

DIXI, which has a PC with 4 active areas that can be independently timed, will be sitting at 6.5 m from TCC (target chamber center) on the NIF (illustrated in figure 2). This is outside the target chamber and pinhole relayed images of the implosion will have a magnification of 64 $\times$. Therefore a field of view of 150 μm at tcc leads to a magnified image of 9.8 mm in diameter and an assumed 10 μm resolution elements will be magnified to 640 μm at the PC. This leads to the need for a large active area on the photo cathode in order to capture enough images for a time sequence. The large size brings with it a number of challenges discussed below. Furthermore, since the system is designed to image the implosions, the instrument has to have a good spatial resolution to only be limited by the spatial resolution of the pinhole imaging system and not by the instrument.

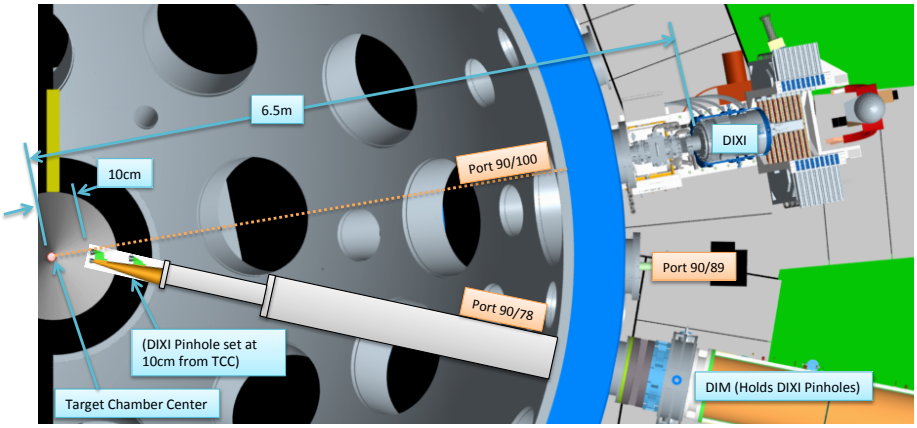

Figure 2. Top view of the equatorial plane on the NIF. DIXI will be situated outside the target chamber, which is indicated by the blue rim.

4. PHOTOCATHODE

4.1 Spatial resolution

The total spatial resolution of the sytem (δ_{tot}) is a convolution of the spatial resolution of the instrument (δ_{instr}) and the resolution of the pinhole imaging system (δ_{ph}).

$$\delta_{\text{tot}} = \sqrt{\delta_{\text{ph}}^2 + \delta_{\text{instr}}^2} \tag{3}$$

How the different spatial resolutions affect the δ_{tot} is summarized for a handful of cases in table 1. This shows that by only improving δ_{instr}, δ_{tot} can be improved significantly (i.e. compare cases A and D in table 1).

The instrument resolution δ_{instr} in turn is determined by the spatial resolution of the PC itself δ_{PC} and the MCP detector δ_{mcp}.

$$\delta_{\text{instr}} = \sqrt{\delta_{\text{PC}}^2 + (\delta_{\text{mcp}} \times \text{Mag}_B)^2} \tag{4}$$

case	δ_{ph} at tcc (μm)	Pinhole size (μm)	Magnification	δ_{ph} at Detector (μm)	δ_{instr} at PC (μm)	δ_{tot} at tcc (μm)
A	10.1	10	64	646	600	13.7
B	10.1	10	64	646	400	11.9
C	7.11	7	64	455	300	8.39
D	10.1	10	64	646	300	11.0

Table 1. Examples of possible spatial resolutions (δ)

The spatial resolution of the gated MCP detector is 45 μm, but because of the de-magnification by the magnetic field translates to $\text{Mag}_B \times \delta_{\text{mcp}} \approx 3{\times}45$ μm at the PC.

δ_{PC} depends on the material of the PC and the magnetic field strength at its position. Secondary photoelectrons are ejected with a characteristic energy spread depending on the PC material. Here we compare CsI and Au as the active PC material. CsI has two distinct advantages over Au, namely it gives a better spatial resolution and also has a higher quantum efficiency (QE), that is more secondary electrons are generated per incident photon.[4] CsI has a characteristic energy spread of 1.7 eV, compared to Au at 3.5 eV.[4] In the solenoid field the transverse excursion of the photoelectrons, and therefore δ_{PC}, is limited to 4 times their cyclotron radius.[1]

$$4r_L[\mu m] = 95000\frac{\sqrt{T_e[eV]}}{B[\text{Gauss}]}. \tag{5}$$

This shows that the spatial resolution is inversely proportional to the magnetic field at the PC. The resulting theoretical instrument resolution using equations 4 and 5 is plotted in figure 3 (lines) for different magnetic fields and the two PC materials.

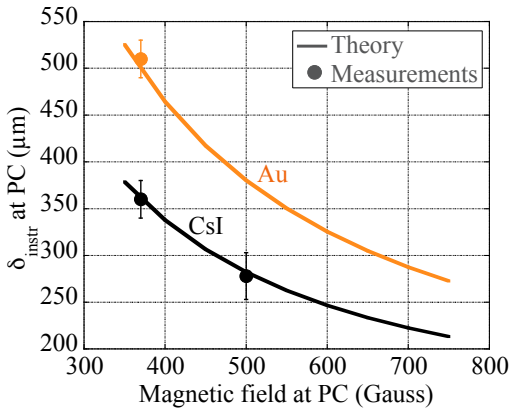

Figure 3. Instrument resolution (δ_{instr}) at the PC plotted against magnetic field strength at the PC for two different PC materials (Au and CsI). The solid symbols show the experimentally measured (10-90% rise) spatial resolutions.

Measurements with a laser generated x-ray source were conducted at the COMET laser at LLNL. The laser had a pulse duration of 500-700 fs, a wavelength of 1.054 μm and a spot size of FWHM 8 μm. This lead to laser intensities around 2×10^{19} Wcm^{-2} that were focused onto a 200 μm Cu target. The generated x-rays had an unobstructed view to the instrument, which was run in pulsed mode, and the strips were nearly co-timed. The spatial resolution of the instrument for the two PC materials was measured. To obtain the spatial resolution, the distance over which the signal level across the edge of a tantalum mask positioned in front of the transmission PC increases from 10-90% is measured. Measurements at 370 Gauss extraction field give a spatial resolution of 360 μm for the CsI PC, and 510 μm for the Au PC. For a CsI PC the magnetic extraction field was increased to 500 Gauss. The corresponding measured resolution is 280 μm. This is in good agreement with the value for δ_{instr} assumed for cases C and D in table 1. All data points are in good agreement with the theory, and are plotted in figure 3. On the NIF CsI will be used as the PC material. In addition to the higher spatial resolution, another advantage of CsI as a PC material over Au is the predicted[4] and widely observed increased quantum efficiency of CsI compared to Au, especially at the higher x-ray energies.

4.2 PC design

The PC design for DIXI is: 50 μm Polyimmide film, with 200 nm Al, the ends of which are coated with 200 nm of Au for better electrical contact, the active PC area is coated with 400 nm of hard (non-fluffy) CsI. The benefit of the fairly thick material is the increased quantum efficiency at around 8-10 keV. Frumkin et al.[6] measured the dependence of the quantum efficiency on the material thickness for CsI PC material and different x-ray energies (figure 10 in reference[6]). Their study found that the QE reaches its maximal value at a CsI thickness of about 300-400 nm, for 5.9 and 8 keV photons, while the optimal thickness for higher x-ray energies is even thicker. They also observed a decrease in QE at thicknesses larger than the optimal, which they attributed to photons being absorbed in the front layers at a distance from the emission surface which is larger than the escape length of the secondary electron cascade. In other words, these layers of the photo convertor just play the role of attenuation of the x-ray flux arriving to the "useful" layers near the emission surface. The benefits of aluminium over gold as the conducting substrate is the higher and more homogeneous transmission of x-rays, especially between 5 and 10 keV . Polyimmide was chosen as the PC substrate because it is an insulator and transmits x-rays.

4.3 PC flatness

As mentioned above, the high magnification of the images on NIF results in the need for a large active area of the photocathode. At the same time it is important to be able to correlate the time of the images across the strip, and therefore have a constant propagation of the HV pulse across the strip. The big active area needed brings with it the challenge of maintaining an even gap between the PC and the anode mesh. This is accomplished by striving to keep the photocathode substrate flat. Figure 4 shows two raw images comparing the effect a wrinkled (b) PC has compared to a flat one (a). The observed distortion of the signal is attributed to the difference in the position of the zero crossing of the HV PC pulse along the strip when the x-rays hit the PC. Whereas the change in drift length due to distorted PC plane is negligible because of the long gate width of the mcp.

5. MECHANICAL PC DESIGN

The flatness of the photo cathode is mainly achieved by improvements made to the mechanical design and tensioning procedure. The photo cathode membrane is bonded to a rigid Macor support

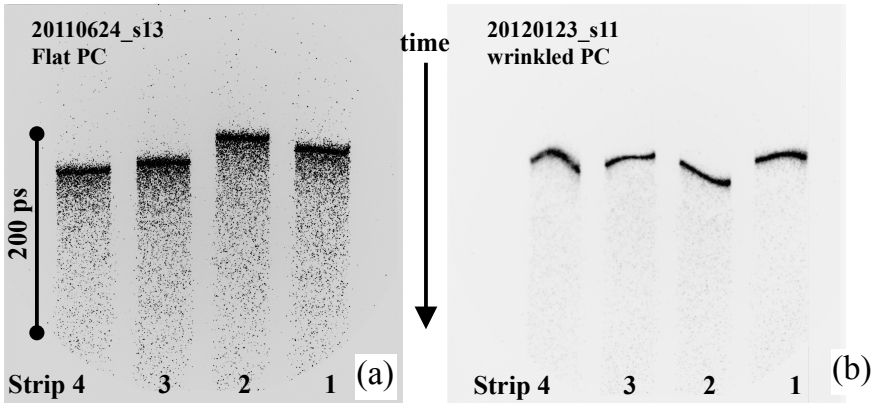

Figure 4. (a) raw DIXI data, signal from a flat PC, transmission Au PC, (b) raw DIXI data, signal from a wrinkled PC, transmission CsI PC. Both cases had a Be window as a filter in front of the PC, and the x-rays were produces by the COMET short pulse laser hitting a Cu target.

ring only sparing the active area of the photo cathode. Macor was chosen because of its high modulus of elasticity, an improvement of 18 × more stiff over the original design using PEEK and a thinner support frame. The low CTE of Macor provides a dimensionally stable platform which is ideal for use as a rigid flat support structure. The photo cathode membrane is tensioned using a thermal hydroscopic tensioning process. The photocathode is stretched over the Macor support ring and bonded around the periphery in an environmental oven at 80°C and 50% humidity. During the cure the CTE mismatch and the swelling of the film due to water absorption creates an ideal condition while the epoxy cures. When the cured photocathode assembly is removed and returned to ambient the membrane shrinks in diameter as its moisture content is reduced. The photocathode tension becomes even tighter during use as the remaining water vapor is driven off the membrane while under vacuum.

6. SUMMARY

In summary we have shown that it is possible to obtain a large area PC that is mechanically flat, which is important to obtain a flat signal and be able to correlate the time of the images across the strip. Furthermore we have measured the spatial resolution of the instrument to be $\delta_{\rm instr}$ <300 μm at the PC and have shown that the magnetic field at the PC can be used to change and improve $\delta_{\rm instr}$.

ACKNOWLEDGMENTS

The Authors would like to acknowledge the support of the staff at the Jupiter Laser Facility and thank the Shape Group or providing the modeling results. Lawrence Livermore National Laboratory is operated by Lawrence Livermore National Security, LLC, for the U.S. Department of Energy, National Nuclear Security Administration under Contract No. DE-AC52-07NA27344.
(LLNL-CONF-566512)

REFERENCES

1. T. J. Hilsabeck et. al., Rev. Sci. Instrum., 81, 10E317, (2010).
2. S. Atzeni and J. Meyer-ter Vehn, The Physics of Inertial Fusion, International Series of Monographs on Physics (Clarendon Press, Oxford, 2004); J. D. Lindl, Inertial Confinement Fusion: The Quest for Ignition and Energy Gain Using Indirect Drive (Springer-Verlag, New York, 1998).
3. D. K. Bradley, P. M. Bell, O. L. Landen, J. D. Kilkenny, and J. Oertel, *Rev. Sci. Instrum.*, **66**, 716 (1995).
4. B.L. Henke, J.P Knauer and K. Premaratne, *J. Appl. Phys.*, **52**(3), 1509 (1981).
5. S. R. Nagel *et. al.*, *Rev. of Sci. Instrum.*, **83**, 10E116 (2012); http://dx.doi.org/10.1063/1.4732849.
6. I. Frumkin *et al.*, *Nuclear Instruments and Methods in Physics Research*, **A329**, 337 (1993).